Transverse-electric and transverse-magnetic waves in nonlinear isotropic waveguides

A. D. Boardman and T. Twardowski
Applied Optics Group, Department of Physics, University of Salford, Salford M5 4WT, United Kingdom
(Received 26 September 1988)

A full theory of the interaction between nonlinear transverse-electric and transverse-magnetic waves is derived. A new form of third-order tensor that accounts for the presence of the two polarizations is described and a mathematical discussion of the first integral is presented. The theory is illustrated by a full set of numerical results both for single-interface and thin-film structures.

I. INTRODUCTION

There is considerable worldwide interest in nonlinear waveguide propagation. This is because of the many advantages that accrue when a waveguide format is used. Among these are the well-known concentration of energy in the plane of thin films and in the core of an optical fiber and the possibility of long interaction lengths. For some time the emphasis was upon weak nonlinearity but, in recent years, there has been a growth in activity on strongly nonlinear guides, in which the changes in the linear refractive indices across material interfaces can be matched to achievable nonlinearities. The principal effort was initially concentrated upon nonlinear TE waves in isotropic media,[1–13] since they are amenable to analytical analysis, but TM waves are now also well understood.[14–22] In all of these calculations, and in the interpretations of experiments, it is assumed that either purely TE or TM waves propagate. An inspection of the nonlinear dielectric tensor for isotropic materials reveals, however, the possibility that both polarizations can propagate simultaneously and that one polarization can sometimes act as a channel for the other.

The question of nonlinear channeling raises a number of interesting and challenging problems, some of which have been addressed before. For example, strong waves can propagate in an otherwise opaque medium through a kind of nonlinear bleaching action.[23] Of more immediate interest is the ability of one strong polarization to create a channel for a weak wave with a different polarization. In particular, the propagation of a weak TM wave in the channel created by a strong TE wave has been considered recently.[24] For this case 100% modulation of the weak wave by the strong beam was predicted. This new development was complemented by a short report of a more general theory[25] which showed that weak-wave propagation in the channel of a strong wave was simply one limit of a whole spectrum of mixed TE-TM stationary states. This theory was based on a nonlinear dielectric tensor appropriate only to thermal nonlinearities. The present paper seeks to present a full report in which the nonlinear TE-TM interaction is given for a more general class of nonlinear dielectric tensor together with a discussion of the first integral and a detailed set of results for thin-film guiding structures.

II. BASIC THEORY

In this problem the interaction of two waves, namely, TE and TM, with different wave numbers p and q but at the same frequency ω is considered. The relevant nonlinear dielectric tensor for isotropic media can be obtained directly from previously published forms of the third-order electric polarization[15] but will be derived here from first principles. This approach shows clearly the modifications that must be made if nonisotropic media are to be considered or if harmonic generation and wave mixing are to be included.

Consider a planar guiding structure whose interfaces lie in the x-y Cartesian plane supporting a surface or guided wave whose wave vector is parallel to the x axis, as shown in Fig. 1.

For a nonlinear medium the third-order electric polarization at position $\mathbf{x}$ and time t can be written as[26]

$$P_i^{(3)}(\mathbf{x},t)=\epsilon_0\int_{-\infty}^{\infty}d\omega_1\int_{-\infty}^{\infty}d\omega_2\int_{-\infty}^{\infty}d\omega_3\int_{-\infty}^{\infty}dk_1\int_{-\infty}^{\infty}dk_2\int_{-\infty}^{\infty}dk_3\chi_{ijkl}^{(3)}(-\omega_1-\omega_2-\omega_3,\omega_1,\omega_2,\omega_3)\times\mathcal{E}_j(\omega_1,k_1)\mathcal{E}_k(\omega_2,k_2)\mathcal{E}_l(\omega_3,k_3)\times e^{i[(k_1+k_2+k_3)x-(\omega_1+\omega_2+\omega_3)t]}\,, \tag{1}$$

where $\chi^{(3)}$ is the spatially independent third-order susceptibility tensor, $\underline{\mathcal{E}}$ is the electric field, and ω_i and k_i are the frequency and wave number, respectively. Now consider the case

$$\underline{\mathcal{E}}(\omega_i,k_i)=[\mathbf{A}\delta(k_i-p)+\mathbf{B}\delta(k_i-q)]\delta(\omega_i-\omega)+\text{c.c.}\,, \tag{2}$$

where

$$\mathbf{A}=(\mathcal{E}_x,0,\mathcal{E}_z) \tag{3}$$

and

$$\mathbf{B}=(0,\mathscr{E}_y,0)\ , \tag{4}$$

i.e., the electric field has a single frequency ω but the TM and TE components have different wave numbers, p and q, respectively. The polarization is then given by

$$\begin{aligned}P_i^{(3)}(\mathbf{x},t)=\epsilon_0\chi_{ijkl}^{(3)}(-\omega_1-\omega_2-\omega_3,\omega_1,\omega_2,\omega_3)&(A_j e^{i(px-\omega t)}+A_j^* e^{-i(px-\omega t)}+B_j e^{i(qx-\omega t)}+B_j^* e^{-i(qx-\omega t)})\\ &\times(A_k e^{i(px-\omega t)}+A_k^* e^{-i(px-\omega t)}+B_k e^{i(qx-\omega t)}+B_k^* e^{-i(qx-\omega t)})\\ &\times(A_l e^{i(px-\omega t)}+A_l^* e^{-i(px-\omega t)}+B_l e^{i(qx-\omega t)}+B_l^* e^{-i(qx-\omega t)})\ ,\end{aligned} \tag{5}$$

where, of course, the arguments of $\chi^{(3)}$ take the values $\pm\omega$. Multiplying out the above gives

$$\begin{aligned}P_i^{(3)}(\mathbf{x},t)=\epsilon_0\chi_{ijkl}^{(3)}(3\omega,-\omega,-\omega,-\omega)&(A_jA_kA_le^{3i(px-\omega t)}+B_jB_kB_le^{3i(qx-\omega t)})\\ &+3\epsilon_0\chi_{ijkl}^{(3)}(3\omega,-\omega,-\omega,-\omega)(A_jA_kB_le^{i[(2p+q)x-3\omega t]}+B_jB_kA_le^{i[(2q+p)x-3\omega t]})\\ &+3\epsilon_0\chi_{ijkl}^{(3)}(\omega,-\omega,-\omega,\omega)[(A_jA_kA_l^*+2A_jB_kB_l^*)e^{i(px-\omega t)}+B_jB_kA_l^*e^{i[(2q-p)x-\omega t]}]\\ &+3\epsilon_0\chi_{ijkl}^{(3)}(\omega,-\omega,-\omega,\omega)[(B_jB_kB_l^*+2B_jA_kA_l^*)e^{i(qx-\omega t)}+A_jA_kB_l^*e^{i[(2p-q)x-\omega t]}]+\text{c.c.}\end{aligned} \tag{6}$$

Equation (6) has been reduced to this relatively simple form by the use of intrinsic permutation symmetry,[26] which requires that $\chi_{ijkl}^{(3)}(-\omega_1-\omega_2-\omega_3,\omega_1,\omega_2,\omega_3)$ is invariant under exchange of the pairs of indices $j\omega_1$, $k\omega_2$, and $l\omega_3$. Neglecting third-harmonic and non-phase-matched terms, Eq. (6) gives

$$P_i^{(3)}=3\epsilon_0\chi_{ijkl}^{(3)}(\omega,-\omega,-\omega,\omega)[(A_jA_kA_l^*+2A_jB_kB_l^*)e^{i(px-\omega t)}+(B_jB_kB_l^*+2B_jA_kA_l^*)e^{i(qx-\omega t)}]\ , \tag{7}$$

where the $(\mathbf{x},t)$ dependence of the polarization and the complex conjugate have been dropped for clarity. Performing the summations over repeated indices in Eq. (7) for an isotropic medium leads to

$$P_x^{(3)}=\epsilon_0[2\chi_{xxyy}(|\mathscr{E}_x|^2+|\mathscr{E}_y|^2+|\mathscr{E}_z|^2)\mathscr{E}_x+\chi_{xyyx}(\mathscr{E}_x^2+\mathscr{E}_z^2)\mathscr{E}_x^*]e^{i(px-\omega t)}\ , \tag{8a}$$

$$P_y^{(3)}=\epsilon_0[2\chi_{xxyy}(|\mathscr{E}_x|^2+|\mathscr{E}_y|^2+|\mathscr{E}_z|^2)\mathscr{E}_y+\chi_{xyyx}\mathscr{E}_y^2\mathscr{E}_y^*]e^{i(qx-\omega t)}\ , \tag{8b}$$

$$P_z^{(3)}=\epsilon_0[2\chi_{xxyy}(|\mathscr{E}_x|^2+|\mathscr{E}_y|^2+|\mathscr{E}_z|^2)\mathscr{E}_z+\chi_{xyyx}(\mathscr{E}_x^2+\mathscr{E}_z^2)\mathscr{E}_z^*]e^{i(px-\omega t)}\ . \tag{8c}$$

It can be seen that χ_{xxyy} describes an "isotropic" part of the nonlinear polarization. This term alone would give a nonlinear refractive index change which is the same in all directions. The coefficient χ_{xyyx} describes an "anisotropic" part of the nonlinear polarization, despite the fact that Eqs. (8) refer specifically to the nonlinear polarization in an *isotropic* medium. Hence the second term gives rise to a nonlinear birefringence. Notice that if the TE and TM components had the same wave number Eqs. (8) would take the form

$$P_i^{(3)}=2\epsilon_0\chi_{xxyy}\mathscr{E}_j\mathscr{E}_j^*\mathscr{E}_i+\epsilon_0\chi_{xyyx}\mathscr{E}_j\mathscr{E}_j\mathscr{E}_i^*\ ,$$

as given in Ref. 15. For a surface or guided wave $\mathscr{E}_x$ and $\mathscr{E}_z$ are $\pi/2$ out of phase with each other.[15] Introducing the substitutions

$$\mathscr{E}_x=iE_x,\quad \mathscr{E}_y=E_y,\quad \mathscr{E}_z=E_z\ , \tag{9}$$

where E_x, E_y, and E_z are all real, and

$$\alpha=2\chi_{xxyy}+\chi_{xyyx}\ , \tag{10}$$

$$\gamma=\frac{2\chi_{xxyy}-\chi_{xyyx}}{2\chi_{xxyy}+\chi_{xyyx}}\ , \tag{11}$$

$$\eta=\frac{2\chi_{xxyy}}{2\chi_{xxyy}+\chi_{xyyx}}\ , \tag{12}$$

allows Eqs. (8) to be written in the very simple form

$$P_x^{(3)}=\epsilon_0\alpha(E_x^2+\eta E_y^2+\gamma E_z^2)E_xe^{i(px-\omega t)}\ , \tag{13a}$$

$$P_y^{(3)}=\epsilon_0\alpha(\eta E_x^2+E_y^2+\eta E_z^2)E_ye^{i(qx-\omega t)}\ , \tag{13b}$$

$$P_z^{(3)}=\epsilon_0\alpha(\gamma E_x^2+\eta E_y^2+E_z^2)E_ze^{i(px-\omega t)}\ , \tag{13c}$$

where $\gamma=\frac{1}{3}$, $-\frac{1}{2}$, and 1, and $\eta=\frac{2}{3}$, $\frac{1}{4}$, and 1 for electronic distortion, molecular orientational, or thermal nonlinear mechanisms, respectively.[15] The dielectric tensor for a nonlinear isotropic material can then be written as

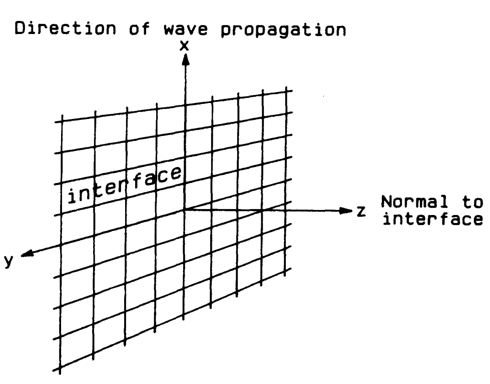

FIG. 1. Geometry of the guiding structure.

$$\underline{\epsilon}=\begin{bmatrix}\epsilon_{xx} & 0 & 0\\ 0 & \epsilon_{yy} & 0\\ 0 & 0 & \epsilon_{zz}\end{bmatrix} \tag{14a}$$

$$=\begin{bmatrix}\epsilon+\alpha(E_x^2+\eta E_y^2+\gamma E_z^2) & 0 & 0\\ 0 & \epsilon+\alpha(\eta E_x^2+E_y^2+\eta E_z^2) & 0\\ 0 & 0 & \epsilon+\alpha(\gamma E_x^2+\eta E_y^2+E_z^2)\end{bmatrix}, \tag{14b}$$

where ϵ is the linear part of the dielectric function. The presence of all three electric field components in each diagonal term causes the TE and TM polarizations to interact with each other. In materials of lower symmetry TE-TM coupling may occur via off-diagonal elements leading to hybrid modes, but this is not appropriate in the present case and hybrid modes do not occur. In general, the stationary mixed TE-TM waves will have associated with them two wave numbers, one for the TE and the other for the TM component, and they must be considered as interacting but *discrete*.

III. FIRST INTEGRAL FOR STATIONARY TE-TM WAVES

The first integral for stationary TE-TM waves can be obtained for the isotropic form of the nonlinear dielectric tensor, Eq. (14), in a similar way to that used for deriving the first integral for TM waves.[17] Maxwell's TM set of equations,

$$\frac{\partial E_x}{\partial z}-pE_z=\omega\mu_0 H_y , \tag{15a}$$

$$\frac{\partial H_y}{\partial z}=-\omega\epsilon_0\epsilon_{xx}E_x , \tag{15b}$$

$$pH_y=-\omega\epsilon_0\epsilon_{zz}E_z , \tag{15c}$$

yields

$$\frac{\partial E_x}{\partial z}\frac{\partial^2 E_x}{\partial z^2}=p^2\left[1-\frac{\epsilon_{zz}}{\beta_{\rm TM}^2}\right]E_z\frac{\partial E_z}{\partial z}-\frac{\omega^2}{c^2}\epsilon_{xx}E_x\frac{\partial E_x}{\partial z} , \tag{16}$$

where $\beta_{\rm TM}=pc/\omega$. Integrated with respect to z this equation gives

$$\frac{c^2}{\omega^2}\left[\frac{\partial E_x}{\partial z}\right]^2+\frac{\alpha}{2}(E_x^4+E_z^4)+\gamma\alpha E_x^2E_z^2+\beta_{\rm TM}^2E_x^2-(\beta_{\rm TM}^2-\epsilon)(E_x^2+E_z^2)=-2\alpha\eta\int(E_y^2E_z dE_z+E_y^2E_x dE_x)+C_{\rm TM} , \tag{17}$$

where $C_{\rm TM}$ is the integration constant.

Maxwell's TE set of equations,

$$\frac{\partial E_y}{\partial z}=\omega\mu_0 H_x , \tag{18a}$$

$$qE_y=\omega\mu_0 H_z , \tag{18b}$$

$$\frac{\partial H_x}{\partial z}-qH_z=-\omega\epsilon_0\epsilon_{yy}E_y , \tag{18c}$$

yield the following differential equation for E_y:

$$\frac{\partial^2 E_y}{\partial z^2}=\left[q^2-\frac{\omega^2}{c^2}\epsilon_{yy}\right]E_y . \tag{19}$$

When integrated with respect to z, this equation gives

$$\frac{c^2}{\omega^2}\left[\frac{\partial E_y}{\partial z}\right]^2-(\beta_{\rm TE}^2-\epsilon)E_y^2+\frac{\alpha}{2}E_y^4=-2\alpha\eta\int(E_x^2E_y dE_y+E_z^2E_y dE_y)+C_{\rm TE} , \tag{20}$$

where once again $C_{\rm TE}$ is the integration constant and $\beta_{\rm TE}=qc/\omega$.

The unresolved integrals in Eqs. (17) and (20) can be evaluated by adding them together, i.e.,

$$2\int E_y^2E_z dE_z+E_y^2E_x dE_x+E_x^2E_y dE_y+E_z^2E_y dE_y=E_x^2E_y^2+E_y^2E_z^2 . \tag{21}$$

This final result gives the following first integral for stationary TE-TM waves:

$$\alpha(\eta E_y^2E_z^2+\eta E_x^2E_y^2+\gamma E_x^2E_z^2)+\frac{\alpha}{2}(E_x^4+E_y^4+E_z^4)+\epsilon(E_x^2+E_y^2+E_z^2)=\beta_{\rm TM}^2E_z^2+\beta_{\rm TE}^2E_y^2-\frac{c^2}{\omega^2}\left[\left[\frac{\partial E_x}{\partial z}\right]^2+\left[\frac{\partial E_y}{\partial z}\right]^2\right]+C_{\rm TM}+C_{\rm TE} . \tag{22}$$

The usual procedure when dealing with surface or guided waves is to set the integration constants to zero. However, it must be noted that for surface or guided waves in linear semi-infinite media (i.e., $\alpha=0$) the constants $C_{\rm TM}$ and $C_{\rm TE}$ must both *separately* be zero in order that all the field components are zero at infinity. This condition must also apply in *nonlinear media* and hence the condition that the sum of $C_{\rm TE}$ and $C_{\rm TM}$ is zero in Eq. (22) is not sufficient because it does not disallow the possibility that $C_{TE} = -C_{TM}$ and that both are finite. For example, the application of single-interface boundary conditions to the first integral for TE-TM waves will yield a continuum of eigenvalues corresponding to the continuum of values that $C_{TE} = -C_{TM}$ can take, with only the eigenvalues corresponding to $C_{TE} = C_{TM} = 0$ being correct. Since it is not possible to treat the two constants separately, the first integral in this case is of very limited value. It can, however, be used as a check on the validity of results obtained from purely numerical calculations.

IV. STATIONARY NONLINEAR TE-TM WAVE REGIONS

The first step in the calculation of TE-TM surface or guided waves is to determine for what range of β_{TE} and β_{TM} values nonlinear stationary waves actually exist. It turns out that this can be done without recourse to a full nonlinear wave calculation. There are obviously no TE-TM waves at a single interface between a metal and a nonlinear dielectric since this supports only TM polarized waves. However, a single interface between a nonlinear and linear medium, shown schematically in Fig. 2, whose dielectric functions are positive, will support both TE and TM polarizations, and hence can permit nonlinear interaction between the two. The important point is that guiding takes place due to the nonlinear formation of a channel of relatively high refractive index in the nonlinear medium. It is then reasonable to assume that the channel formed by, for example, a nonlinear TE wave would, if somehow "frozen" into the nonlinear medium, be able to support a *linear* TM wave with an eigenvalue related (via the shape and size of the channel) to the nonlinear eigenvalue of the TE wave. Such a scenario corresponds in practice to a nonlinear TE wave and a zero-amplitude nonlinear (i.e., effectively linear) TM wave propagating simultaneously along a single interface. The TM wave is guided by the channel created by the TE wave, but the TE wave is unaffected by the TM wave because of the zero amplitude of the TM field components. It is therefore possible on the β_{TE} and β_{TM} plane to draw a locus that represents a pure nonlinear TE wave and a zero-amplitude TM wave. There is also a second locus which corresponds to a pure nonlinear TM wave and a

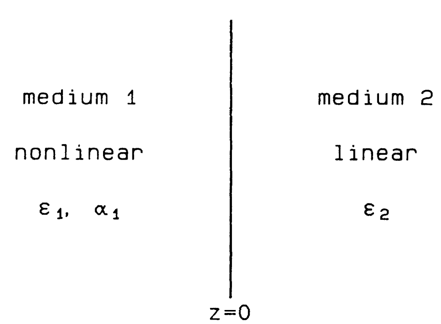

FIG. 2. Schematic of single-interface guiding structure: $\epsilon_2 > \epsilon_1 > 0$, $\alpha_1 > 0$.

zero-amplitude TE wave. Solutions to Maxwell's equations should be found within the area between the two loci and these are the desired stationary TE-TM nonlinear surface and guided waves. Points outside this region correspond to nonstationary states and these will not be considered here.

The two loci on the β_{TE} and β_{TM} plane which delineate the region of stationary nonlinear TE-TM waves can therefore be found by incorporating an expression for the nonlinear guiding channel created by one polarization into the linear dielectric function used to calculate the linear eigenvalue of the other polarization. For example, the dielectric tensor for the half space $z<0$ used in calculating the linear eigenvalue of TM waves in a TE-induced channel has the form

$$\underline{\epsilon} = \begin{bmatrix} \epsilon_1 + \alpha_1 \eta E_y^2(z) & 0 \\ 0 & \epsilon_1 + \alpha_1 \eta E_y^2(z) \end{bmatrix} , \tag{23}$$

where

$$E_y^2(z) = \frac{\kappa_{TE,1}^2}{\Lambda \cosh^2[\kappa_{TE,1}(z - z_0)]} , \tag{24}$$

$$\Lambda = \frac{\omega^2 \alpha_1}{2c^2} , \tag{25}$$

$$\tanh(\kappa_{TE,1} z_0) = -\frac{\kappa_{TE,2}}{\kappa_{TE,1}} , \tag{26}$$

and

$$\kappa_{TE,n}^2 = \frac{\omega^2}{c^2} (\beta_{TE}^2 - \epsilon_n) , \tag{27}$$

where the subscript n refers to medium n. The corresponding dielectric tensor for a TM-induced channel cannot be expressed analytically, but, by solving the TM wave equations, can be generated numerically in the same form as the tensor (23). The linear eigenvalues for this modified structure can then be calculated using standard ordinary differential equation software.[27]

Sample results are presented in Fig. 3, which shows the region on the β_{TE}-β_{TM} plane in which nonlinear TE-TM stationary states occurs for a single interface between N-(p-methoxybenzylidene-p-butylaniline) (MBBA) (with a thermal nonlinearity, $\gamma = \eta = 1$) and a linear dielectric with $\epsilon = 2.5$. The two loci converge to a point at $\beta_{TE}^2 = \beta_{TM}^2 = \epsilon_2$, below which the nonlinear waves become oscillatory in the linear dielectric and the power flow becomes infinite. It is clear that, with the possible exception of the low-β cutoff point, no stationary TE-TM wave solutions exist for $\beta_{TE} = \beta_{TM}$. This confirms that in the stationary TE-TM wave the two polarizations maintain their separate identities by having different guided wavelengths. As could be expected, this type of interaction is unique to nonlinear waves since it is due purely to the nonlinear terms in the dielectric function. The inset in Fig. 3 shows the region around $\beta_{TE} = 1.582$ on a very much expanded scale. The upper locus shows the linear eigenvalues of TM waves in the presence of a nonlinear TE wave, and the lower locus describes zero-amplitude TE waves in a structure modified by a nonlinear TM

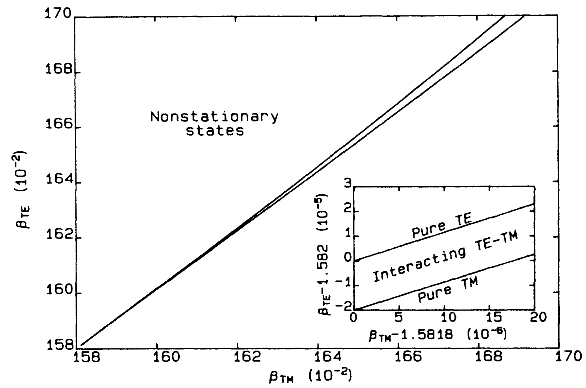

FIG. 3. The β_{TE}-β_{TM} plane for nonlinear surface guided waves at a single interface between MBBA liquid crystal with $\epsilon_1=2.4025$, $\alpha_1=6.379\times10^{-12}$ m^2V^{-2} and a linear dielectric with $\epsilon_2=2.5$ at $\omega=3.658\times10^{15}$ rad s^{-1}. The lower curve is the locus of linear TE eigenvalues in a channel created by a nonlinear self-focused TM wave and the upper curve the locus of linear TM eigenvalues in a nonlinear TE channel. Stationary interacting TE-TM states exist in the region between the two loci. The inset shows the region around $\beta_{TE}=1.582$ on a very much expanded scale.

wave.

The possibility for the existence of stationary nonlinear TE-TM waves increases greatly if a thin metal film or dielectric layer is inserted between the nonlinear medium and linear dielectric, as shown in Fig. 4. To gain a proper understanding of the nonlinear interactions that may occur, the stationary states of pure nonlinear TE and TM waves in the thin-film structure must be known. These eigenvalues are discussed in detail in the Appendix.

For the thin-metal-film structure it is clear that in order to get nonlinear TE-TM stationary states the metal-film thickness must be below the critical value for the existence of TE plasmons. Figure 5 shows the loci on the β_{TE}-β_{TM} plane between which there exist stationary TE-plasmon–pseudoplasmon states, that should be compared to the stationary TE-TM states at a single interface. In contrast with the single-interface results, the loci are finite. Both loci meet the low-β_{TE} cutoff point before reaching the low-β_{TM} cutoff, implying that for low values of β_{TM} the guiding channel created by the pseudoplasmon is not large enough to support a zero-amplitude TE wave.

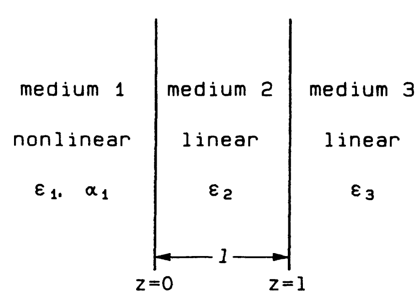

FIG. 4. Schematic of the layered guiding structure. For the thin-metal-film case $\epsilon_3>\epsilon_1>0$, $\epsilon_2<0$ and for the dielectric-layer case $\epsilon_2>\{\epsilon_1,\epsilon_3\}>0$.

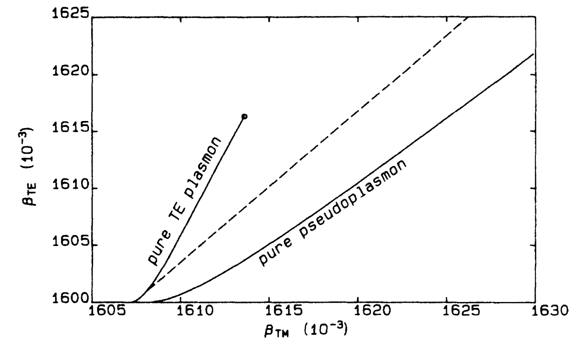

FIG. 5. The β_{TE}-β_{TM} plane for nonlinear self-focused waves in a thin-metal-film structure at $\omega=3.658\times10^{15}$ rad s^{-1} with MBBA as the nonlinear medium, $\epsilon_2=-10$ (Al), $\epsilon_3=2.56$, and $l=1.5$ nm. The curve labeled pure TE plasmon is the locus of TM linear eigenvalues in a nonlinear TE-plasmon channel and the curve labeled pure pseudoplasmon is the locus of TE linear eigenvalues in a nonlinear pseudoplasmon channel. The cutoff point for pure TE plasmons is circled. The dashed line is referred to in Fig. 8.

Hence the stationary states along the line joining the two loci at the low-β_{TE} cutoff will consist of mixed TE-TM states.

The locus of linear short-range plasmon eigenvalues in the presence of a nonlinear TE plasmon is shown in Fig. 6. Nonlinear stationary TE-plasmon–short-range-plasmon states exist in the region to the right of the pure TE locus. Increases in the value of β_{TE} result in a decrease in the TE-TM interaction due to the movement of the self-focused peak of the TE wave away from the interface: the upper cutoff of the pure TE locus gives the linear eigenvalue of short-range plasmons in the absence of the nonlinear TE wave, for which at this point the self-focused peak has moved an infinite distance from the metal film. This time there is no locus corresponding to nonlinear short-range plasmons with zero-amplitude TE plasmons since the short-range plasmons do not form a

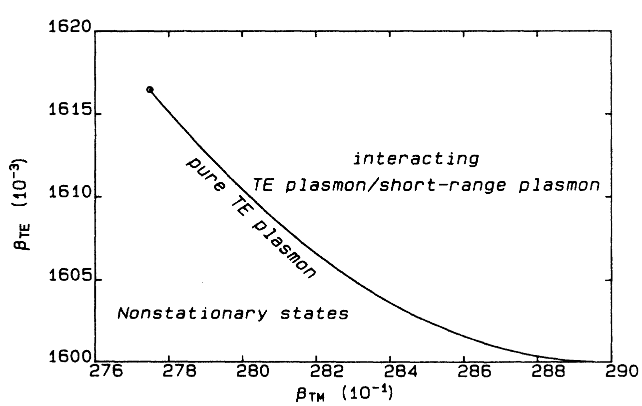

FIG. 6. Locus of linear short-range plasmon eigenvalues in a nonlinear TE-plasmon channel for the MBBA/Al/linear-dielectric structure of Fig. 5. The circle marks the pure TE-plasmon cutoff point and the linear eigenvalue of pure short-range plasmons.

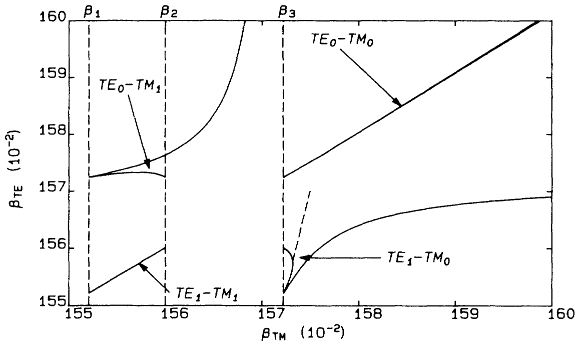

FIG. 7. The β_{TE}-β_{TM} plane showing regions of stationary interacting nonlinear guided modes in a dielectric-layer structure. The nonlinear medium is MBBA, $\epsilon_2=2.5$, $\epsilon_3=2.4025$, $l=1$ μm with other data as for Fig. 5. β_1 is the linear eigenvalue of the TM_1 mode, β_2 is its nonlinear cutoff, and β_3 is the linear eigenvalue of the TM_0 mode. The dashed line in the TE_1-TM_0 stationary-state region is referred to in Fig. 11.

guiding channel and therefore cannot support zero-amplitude TE waves.

Figure 7 shows the loci on the β_{TE}-β_{TM} plane delineating the regions of stationary TE-TM waves in the dielectric layer structure. For the data used, only the two lowest-order guided modes exist and this leads to four regions of interaction, namely, TE_0-TM_0, TE_0-TM_1, TE_1-TM_0, and TE_1-TM_1. The loci corresponding to pure TM_0 and TE_0 modes increase without limit, while those corresponding to pure TM_1 and TE_1 have a cutoff. In principle, this configuration can support the greatest number of different regions of nonlinear TE-TM stationary states. Notice that the locus of linear eigenvalues of TM_0 modes in a TE_1 channel begins and ends with the same value of β_{TM}: at the lower value of β_{TE} the TE_1 mode has zero amplitude and at the upper value the self-focused peak of the TE_1 mode has moved out to infinity. Hence in both limits there is no nonlinear TE-TM interaction and therefore β_{TM} is the same. For interacting TE_0-TM_1 stationary waves it is β_{TE} that has the same value at the two extremes of the pure TM locus. The TE_1-TM_1 region is infinitely narrow within the limits of numerical accuracy and it appears that stationary interacting TE_1-TM_1 states do not in fact exist in this case.

V. FULL NONLINEAR INTERACTING WAVE CALCULATIONS

To perform the numerical calculations, a finite-z range equal to ζ must be chosen of sufficient length to allow the field solution components to approximate their asymptotic values very closely. The boundary conditions at infinity are then applied at ζ instead. The numerical algorithm[25] consists of a root-finding loop for the TM waves nested within a root-finding loop for the TE waves. A pair of values for β_{TE} and β_{TM} is first chosen from within the stationary-state regions calculated in Sec. IV. The program then iterates around the loops, varying the field amplitudes at the interfaces, until a self-consistent interacting TE-TM eigenvalue solution is found. Such a calculation would in general produce a power-flow surface characterized by the two wave numbers, β_{TE} and β_{TM}. However, because of the computational size of the problem a more reasonable approach is to calculate only selected power-flow curves for sections through the power-flow surface. The power-dispersion curves and field profiles for interacting TE-TM waves at a single interface have been reported before[25] and we will concentrate on the thin-film case here.

Figure 8 shows a sample power-dispersion curve for interacting TE-plasmon–pseudoplasmon stationary states. The variation of the β_{TE} and β_{TM} values is shown by the dashed line of Fig. 5. The dispersion curve starts on the pure TE-plasmon locus and hence initially the power flow is due entirely to the TE plasmon. As the wave numbers are increased away from the pure TE-plasmon locus a contribution from the pseudoplasmon to the total power flow is introduced. The figure also shows the pure TE-plasmon and pseudoplasmon power-dispersion curves for comparison. It should be noted that the stationary TE-plasmon–pseudoplasmon states can exist for values of β_{TE} above the pure TE-plasmon cutoff point. Hence in principle the pseudoplasmon could be used to switch the TE plasmon between transmitting (stationary) and nontransmitting (nonstationary) states.

The interaction between TE plasmons and short-range plasmons is quite different from that described above. Figure 9 shows the power carried by a short-range plasmon interacting with a TE plasmon as a function of β_{TM} for a fixed value of β_{TE}, and compares it to the power carried by a pure short-range plasmon in the same guiding structure. Also shown is the power flow carried by a pure short-range plasmon if the linear part of the nonlinear dielectric function is $\epsilon_1=2.58$ instead of 2.4025. It is clear that in this case the effect of the nonlinear interaction on the short-range plasmon is a shift in the effective value of the linear part of the nonlinear dielectric function seen by it. Figure 10 shows the power carried by a TE plasmon interacting with a short-range

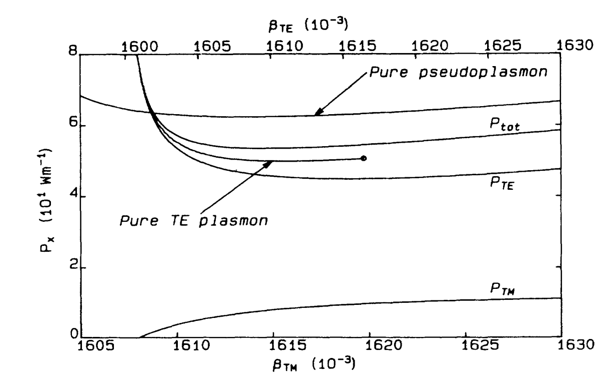

FIG. 8. Power flow of interacting TE-plasmon–pseudoplasmon for values of β_{TE} and β_{TM} shown by the dashed line in Fig. 5. P_{tot}, P_{TE}, and P_{TM} refer to the total power flow and the contributions from the TE plasmon and pseudoplasmon, respectively. Also shown is the power carried by pure TE plasmons and pseudoplasmons. The circle marks the cutoff point for TE plasmons; the cutoff for pseudoplasmons lies off the scale of the figure.

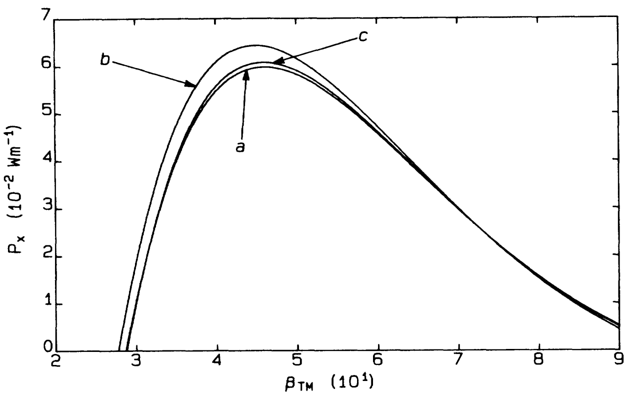

FIG. 9. Power flow as a function of β_{TM} for short-range plasmons in the MBBA/Al/linear-dielectric structure with data as in Fig. 5. The curve labeled a gives the power flow of short-range plasmons interacting with TE plasmons at $\beta_{TE}=1.601$. The curves labeled b and c give the power flow of pure short-range plasmons, but for c, $\epsilon_1=2.58$ is used instead of $\epsilon_1=2.4025$.

plasmon as a function of β_{TM} for fixed β_{TE}. At the low-β_{TM} threshold the short-range plasmon has zero amplitude and hence the power carried by the TE wave is that of a pure TE plasmon. As β_{TM} is increased and the TM field amplitudes grow, the TE power increases at first but then begins to fall off again. This is due to the fact that as β_{TM} is increased, the short-range-plasmon fields not only increase in amplitude but also become more localized at the surfaces of the metal film. Hence the effect of the initial increase of the TM field components on the nonlinear dielectric function seen by the TE plasmon is reversed by their confinement as β_{TM} is increased further.

The differences between the effects observed in stationary TE-plasmon–pseudoplasmon states and TE-plasmon–short-range-plasmon states can be accounted for in terms of the different interaction length scales involved in the two cases. For TE-plasmon–pseudoplasmon interaction the fields of the two polarizations extend to roughly the same distance from the metal film, whereas for TE-plasmon–short-range-plasmon interaction the TE and TM components extend over length scales differing by roughly two orders of magnitude.[25]

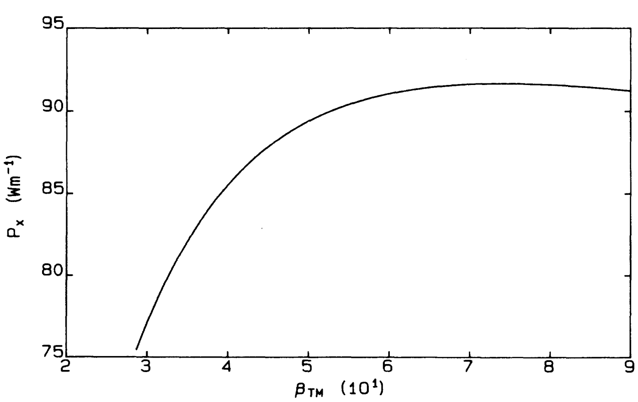

FIG. 10. Power flow for TE plasmons at $\beta_{TE}=1.601$ interacting with short-range plasmons in the MBBA/Al/linear-dielectric structure with data as for Fig. 5.

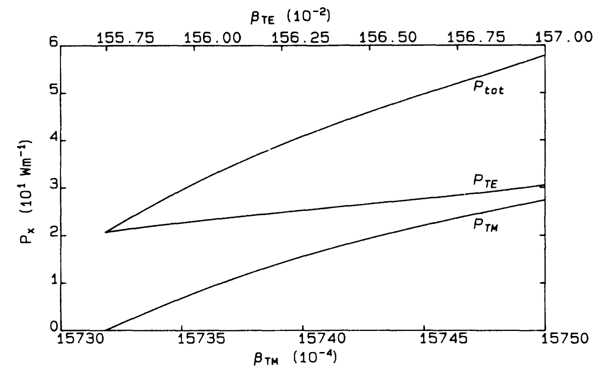

FIG. 11. Power flow for interacting TE_1-TM_0 waves in the dielectric-layer structure for values of β_{TE} and β_{TM} lying along the dashed line in Fig. 7. The data are as for Fig. 7. The curves labeled P_{tot}, P_{TE}, and P_{TM} give the total power flow and the contributions from the TE_1 and TM_0 modes, respectively.

Figure 11 shows the power flow for interacting TE_1-TM_0 stationary states for values of β_{TE} and β_{TM} that lie on the dashed line in Fig. 7. Once again, interacting states exist for values of β_{TE} well above the normal cutoff for pure nonlinear TE_1 waves and hence in principle the TM_0 wave could be used for switching the TE_1 wave "on" and "off." (Similarly, TE_0 waves could be used to switch TM_1 waves.) The evolution of the TE and TM field profiles with increasing total power is shown in Fig. 12. Notice that as the self-focused peak of the TE_1 wave moves away from the dielectric layer, it creates a separate nonlinear guiding channel that causes the peak in the TM_0 field amplitude to split into two separate peaks. At the same time the TM_0 components distort the effective

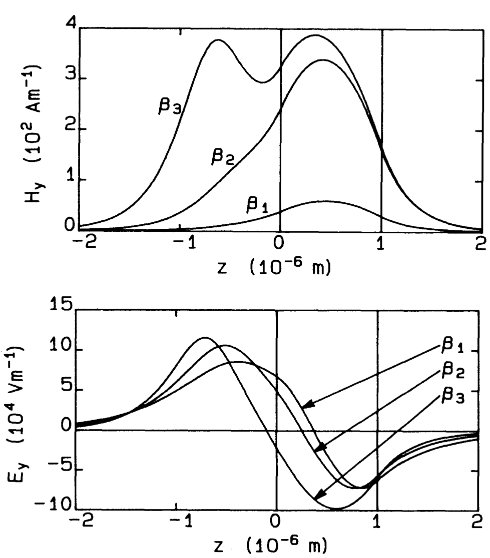

FIG. 12. Field profiles for interacting TE_1-TM_0 modes for increasing values of β_{TE} and β_{TM}. β_1, β_2, and β_3 refer to ($\beta_{TE}=1.558$, $\beta_{TM}=1.573$), ($\beta_{TE}=1.562$, $\beta_{TM}=1.574$), and ($\beta_{TE}=1.570$, $\beta_{TM}=1.575$), respectively.

TABLE I. Analytical results for TM polarized waves in a metal-film structure with one nonlinear bounding medium.

$-\infty<z<0$	Field solutions $0<z<l$	$l<z<\infty$
E_{x0}, H_{y0} (obtained numerically)	$E_x=\frac{\kappa_2}{\omega\epsilon_0\epsilon_2}(be^{-\kappa_2 z}-ae^{\kappa_2 z})$ $H_y=ae^{\kappa_2 z}+be^{-\kappa_2 z}$	$E_x=\frac{\kappa_3}{\omega\epsilon_0\epsilon_3}H_{yl}e^{-\kappa_3(z-l)}$ $H_y=H_{yl}e^{-\kappa_3(z-l)}$
	Boundary conditions At $z=0$	At $z=l$
$\Delta H_y=0$	$H_{y0}=a+b$	$ae^{\kappa_2 l}+be^{-\kappa_2 l}=H_{yl}$
$\Delta E_x=0$	$E_{x0}=\frac{\kappa_2}{\omega\epsilon_0\epsilon_2}(b-a)$	$\frac{\kappa_2}{\epsilon_2}(be^{-\kappa_2 l}-ae^{\kappa_2 l})=\frac{\kappa_3}{\epsilon_3}H_{yl}$

$$\frac{E_{x0}}{H_{y0}}=\frac{\kappa_2[\kappa_2\epsilon_3\tanh(\kappa_2 l)+\kappa_3\epsilon_2]}{\omega\epsilon_0\epsilon_2[\kappa_2\epsilon_3+\kappa_3\epsilon_2\tanh(\kappa_2 l)]} \qquad \text{(T1)}$$

index seen by the TE_1 wave, allowing the amplitude of E_y to change sign in the nonlinear medium. It is this completely new phenomenon of symmetry breaking inside the nonlinear medium that allows the TE_1 wave to exist above its normal cutoff point and the same effect comes into play with all nonlinear interacting TE-TM stationary states.

In summary, this paper has described in detail a host of completely new phenomena that are due to the nonlinear interaction between TE and TM polarizations. The effects have no linear analog and have great potential for use in optical device applications.

ACKNOWLEDGMENTS

A.D.B. wishes to acknowledge support from NATO Research Grant No. RG86/0H7H. T. T. acknowledges support from the University of Salford.

APPENDIX: NONLINEAR EIGENVALUES OF THIN-FILM STRUCTURES

1. Metal film

The analytical solutions for a metal-film structure with one nonlinear bounding medium are given in Tables I and II for TM and TE polarized waves. These will be used in the following discussion to obtain several analytical results.

In general, a thin metal film sandwiched between semi-infinite linear dielectrics supports two TM eigenvalue solutions. For the higher eigenvalue β the amplitude of the transverse-electric field component E_z changes sign in the film, while for the lower eigenvalue it is the longitudinal field component E_x that changes sign inside the film. In a symmetric or nearly symmetric structure, the

TABLE II. Analytical results for TE polarized waves in a metal-film structure with one nonlinear bounding medium.

$-\infty<z<0$	Field solutions $0<z<l$	$l<z<\infty$
$H_x=-\frac{\kappa_1^2\sinh[\kappa_1(z-z_0)]}{\omega\mu_0\sqrt{\Lambda_1}\cosh^2[\kappa_1(z-z_0)]}$ $E_y=-\frac{\kappa_1}{\sqrt{\Lambda_1}\cosh[\kappa_1(z-z_0)]}$	$H_x=\frac{\kappa_2}{\omega\mu_0}(ae^{\kappa_2 z}-be^{-\kappa_2 z})$ $E_y=ae^{\kappa_2 z}+be^{-\kappa_2 z}$	$H_x=-\frac{\kappa_3}{\omega\mu_0}E_{yl}e^{-\kappa_3(z-l)}$ $E_y=E_{yl}e^{-\kappa_3(z-l)}$
	Boundary conditions At $z=0$	At $z=l$
$\Delta H_x=0$	$\frac{\kappa_1^2\sinh(\kappa_1 z_0)}{\sqrt{\Lambda_1}\cosh^2(\kappa_1 z_0)}=\kappa_2(a-b)$	$\kappa_2(be^{-\kappa_2 l}-ae^{\kappa_2 l})=\kappa_3 E_{yl}$
$\Delta E_y=0$	$\frac{\kappa_1}{\sqrt{\Lambda_1}\cosh(\kappa_1 z_0)}=a+b$	$ae^{\kappa_2 l}+be^{-\kappa_2 l}=E_{yl}$

$$\tanh(\kappa_1 z_0)=-\frac{\kappa_2[\kappa_2\tanh(\kappa_2 l)+\kappa_3]}{\kappa_1[\kappa_2+\kappa_3\tanh(\kappa_2 l)]} \qquad \text{(T2)}$$

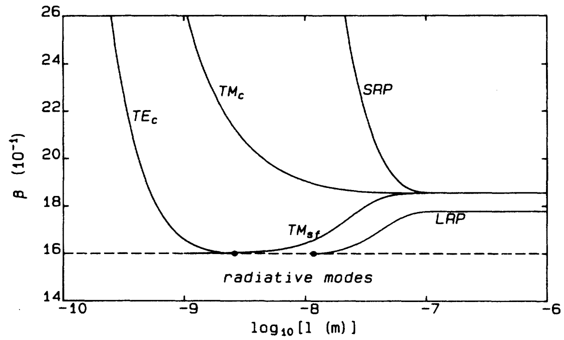

FIG. 13. The effects of film thickness on the waves supported by the MBBA/Al/linear-dielectric structure. The curves labeled SRP and LRP are the linear eigenvalues of short- and long-range plasmons, respectively, TM_c and TE_c are the loci of the cutoff points of pseudoplasmons and TE plasmons, respectively, and TM_{sf} is the locus of values of β at which self-focusing of long-range plasmons and pseudoplasmons sets in. The material data are as for Fig. 5.

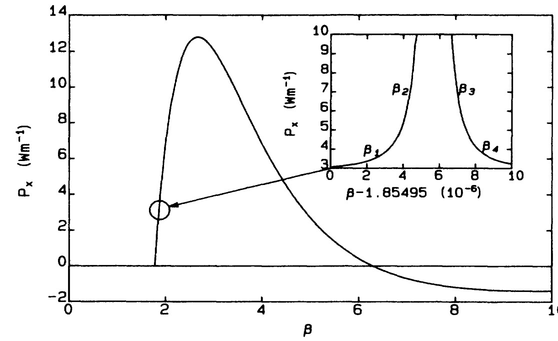

FIG. 15. Power-flow curve for nonlinear long-range plasmon in the MBBA/Al/linear-dielectric structure with an aluminum-film thickness of 0.3 μm. The inset shows the power flow in the vicinity of the short-range plasmon linear eigenvalue, $\beta \simeq 1.85495$, on a very much expanded scale. The points labeled β_1–β_4 are referred to in Fig. 16.

former has a relatively large attenuation coefficient compared to the latter and hence the two eigenmodes are usually referred to as short- and long-range plasmons, respectively.[28] The linear eigenvalues of short- and long-range plasmons are shown in Fig. 13 as a function of the metal-film thickness. It can be seen that in theory short-range plasmons exist for all film thickness, while long-range plasmons exist only above a critical film thickness. In the limit of very large film thicknesses the short- and long-range plasmons degenerate into single-interface surface-plasmon polaritons at the two interfaces.

If one of the bounding media is nonlinear, then nonlinear short- and long-range plasmons are obtained. Figure 14 shows power-dispersion curves for nonlinear short-range plasmons at three different film thicknesses for an MBBA/Al/dielectric structure. These have the same characteristic maximum and reversal in the power flow as single-interface surface-plasmon polaritons. As the film thickness is decreased, the linear eigenvalue increases and the maximum in the power flow decreases. However, the power-flow curves tend to converge at higher values of β since the fields at the two interfaces decouple as their confinement increases.

The nonlinear long-range-plasmon power-dispersion curve for the same structure in the large-film-thickness limit is shown in Fig. 15. Its linear eigenvalue is lower than that of the short-range plasmon and hence as the power flow is increased, the normalized wave number β passes through the linear short-range-plasmon eigenvalue. At this point the power flow becomes infinite as shown in the inset of Fig. 15. The width of this "spike" in the power-dispersion curve decreases with increasing film thickness until it becomes a δ function at infinite film thickness. Hence in this limit, the power-dispersion curve of a nonlinear surface-plasmon polariton at the MBBA/Al interface is recovered. The reason for the spike in the power-flow curve is a sudden increase, followed by a discontinuous sign change, in the field amplitudes at the metal/linear-dielectric interface. This is shown in Fig. 16 as a series of field profiles for four values of β close to the linear short-range-plasmon eigenvalue.

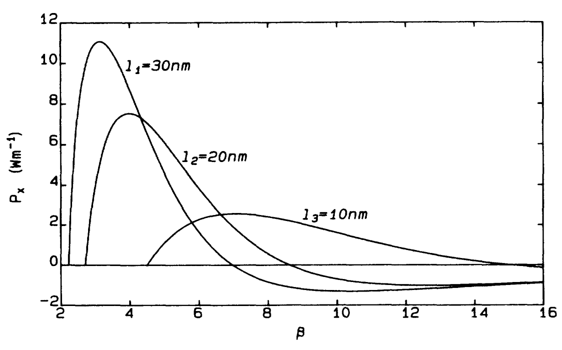

FIG. 14. Power-flow curves for nonlinear short-range plasmons in the MBBA/Al/linear-dielectric structure. The curves are labeled with film thickness. Other data as for Fig. 5.

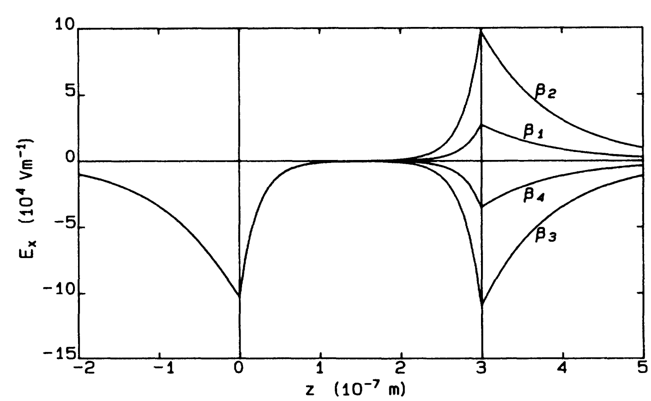

FIG. 16. Field profiles for nonlinear long-range plasmon in the MBBA/Al/linear-dielectric structure with a film thickness of 0.3 μm at values of β near the linear short-range plasmon eigenvalue. The curves labeled β_1–β_4 correspond to points β_1–β_4 in the inset of Fig. 15.

Just below the linear eigenvalue, the field profiles have the type of distribution associated with long-range plasmons, i.e., the electric field component E_x changes sign in the metal film. As β is slightly increased, the field amplitudes at the linear interface blow up and then change sign, taking on a short-range-plasmon-type distribution. It is interesting that throughout this process the field amplitudes at the interface between the metal and nonlinear medium remain unaffected. This then is a very localized linear effect at the linear surface-plasmon eigenvalue, superposed on the broader features of the nonlinear surface plasmon.

From the above discussion it is clear that in the nonlinear case the labels long- and short-range plasmon are no longer appropriate since there is a continuous change in the attenuation coefficient of the wave as the power is increased. However, it is still useful to retain the labels with the understanding that they refer to the linear limit of the nonlinear wave.

An important change to the nonlinear long-range-plasmon characteristics occurs as the metal-film thickness is decreased. Figure 17 shows power-dispersion curves for a series of decreasing thicknesses. First an upper-β cutoff is introduced. Reducing the film thickness still further below the range of existence of linear long-range plasmons introduces a new kind of plasmon with a minimum power threshold, which degenerates into a single-interface self-focused wave as the film thickness is reduced to zero.

In terms of the field distributions this behavior can be explained as follows. For values of β near the long-range plasmon linear eigenvalue the field profiles have the normal type of long-range-plasmon distribution. However, as the wave number β is increased, a self-focused peak forms in the nonlinear medium and moves away from the interface with the metal film, causing a surge in the power flow. This is shown in Fig. 18 as a sequence of field distributions for increasing values of β. The wave eventually cuts off when the self-focused peak has moved out an infinite distance from the metal film.

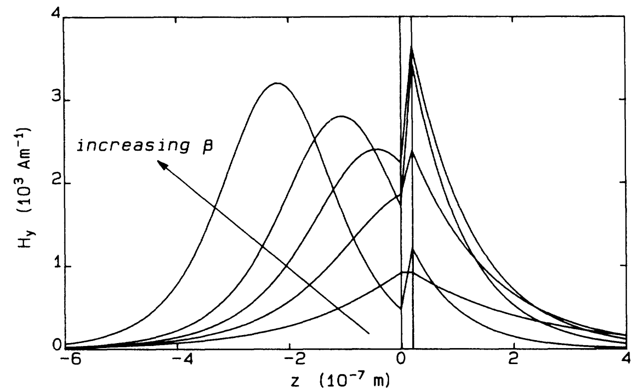

FIG. 18. Evolution of the field profiles of nonlinear long-range plasmons in the MBBA/Al/linear-dielectric structure with a film thickness of 20 nm as β is increased towards its upper cutoff. The curves correspond to $\beta=1.643$, 1.703, 1.763, 1.813, and 1.863.

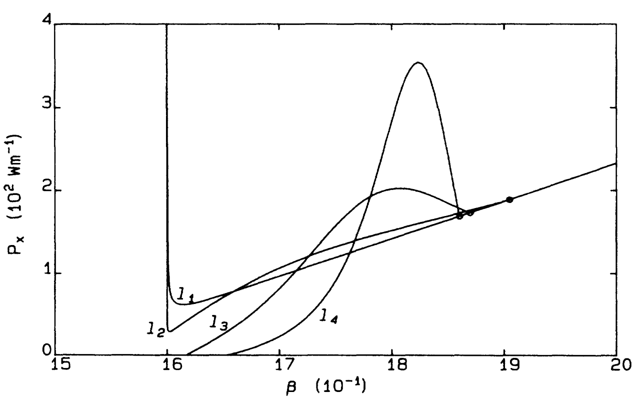

FIG. 17. Evolution of the power flow vs β dispersion curves for TM waves in the MBBA/Al/linear-dielectric structure as the aluminum-film thickness is reduced to zero. The curve labeled l_1 corresponds to $l=0$, i.e., a self-focused wave at the single interface between MBBA and a linear dielectric with $\epsilon=2.56$. l_2, l_3, and l_4 correspond to film thicknesses of 10, 20, and 30 nm, respectively. Other data as for Fig. 5.

Decreasing the film thickness still further to values which no longer support linear long-range plasmons has no effect on the form of the field profiles other than introducing a minimum into the field amplitudes at the interfaces; this is responsible for the formation of the minimum power threshold. From this behavior it is clear that, as the metal-film thickness is decreased, there is a continuous transition from single-interface nonlinear long-range plasmons to self-focused TM waves, via nonlinear long-range plasmons with an upper-β cutoff. Because of the close similarity of self-focused TM waves in a metal-film structure to nonlinear long-range plasmons, the self-focused waves have been named "pseudoplasmons."[25]

Although the power-dispersion curves must be found numerically, the onset of self-focusing and the cutoff point for nonlinear long-range plasmons and pseudoplasmons can be found analytically. The onset of self-focusing corresponds to $E_x=0$ at the nonlinear-medium/metal interface. From Table I this is given by

$$\tanh(\kappa_2 l)=-\frac{\kappa_3\epsilon_2}{\kappa_2\epsilon_3} . \tag{A1}$$

The upper cutoff can be obtained by matching the field ratio given in Table I [Eq. (T1)] to that obtained from the nonlinear TM first integral [Eq. (17)]. Since the cutoff point corresponds to the self-focused peak of the wave being an infinite distance from the metal film, the field amplitudes at the nonlinear-medium/metal-film interface must be zero and hence only the lowest-order terms in Eq. (17) need be retained. Setting E_y and C_{TM} to zero then gives

$$(\beta^2-\epsilon_1)E_{z0}^2=\beta^2E_{x0}^2 \tag{A2}$$

or, substituting for E_z in terms of H_y from Eq. (15c),

$$\frac{E_{x0}}{H_{y0}}=\pm\frac{\kappa_1}{\omega\epsilon_0\epsilon_1} , \tag{A3}$$

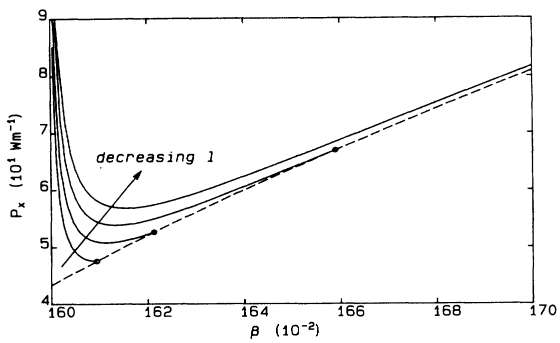

FIG. 19. Power flow as a function of β for TE plasmons in the MBBA/Al/linear-dielectric structure. The curves correspond to aluminum-film thicknesses of 0, 1.0, 1.4, and 1.7 nm, respectively, with circles showing the cutoff points. The dashed line gives the locus of the power flow at cutoff as given by Eq. (A6).

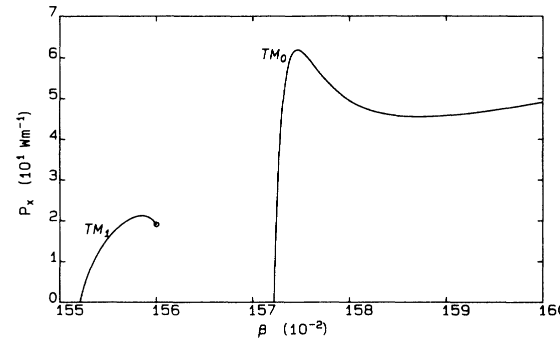

FIG. 20. Power-dispersion curves for nonlinear TM_0 and TM_1 modes in the dielectric-layer structure. The cutoff of the TM_1 mode is circled; the TM_0 mode has no cutoff. Data as for Fig. 7.

where the subscript 0 refers to amplitudes at the nonlinear-medium/metal-film interface. Equating the positive root of Eq. (A3) with Eq. (T1) gives the following expression for the cutoff:

$$\tanh(\kappa_2 l)=\frac{\kappa_2\epsilon_2(\kappa_1\epsilon_3-\kappa_3\epsilon_1)}{\kappa_2^2\epsilon_1\epsilon_3-\kappa_1\kappa_3\epsilon_2^2} . \tag{A4}$$

Since the above equation does not contain any nonlinear parameters, the cutoff is independent of the magnitude and mechanism of the nonlinearity. This is an interesting point in view of the fact that at the cutoff point the waves are very highly nonlinear.

The loci given by Eqs. (A1) and (A4) are shown in Fig. 13 as a function of film thickness. Notice that as the film thickness is reduced to zero, the cutoff point increases to infinity and the onset of self-focusing meets the lower-β threshold for the existence of surface or guided waves. This is consistent with the properties of a single-interface self-focused nonlinear TM wave. For large film thicknesses, both lines converge onto the linear eigenvalue of the short-range plasmon.

Interestingly, Eq. (T1) and the negative root of Eq. (A3) lead to the linear dispersion relations of long- and short-range plasmons since these have identical boundary conditions to those used above for the self-focused waves at cutoff (i.e., field amplitudes which are zero at infinity and tending to zero at the metal-film interfaces).

There is a TE equivalent of the pseudoplasmon which exists over a limited range of film thicknesses and has been termed a TE plasmon in the literature.[29–31] In this case the position of the self-focused peak is given by Eq. (T2) in Table II. Hence the locus of TE-plasmon cutoff, obtained by setting $z_0=-\infty$, is given by

$$\tanh(\kappa_2 l)=\frac{\kappa_2(\kappa_1-\kappa_3)}{\kappa_2^2-\kappa_1\kappa_3} . \tag{A5}$$

This is shown in Fig. 13 as a function of film thickness. The critical film thickness above which TE plasmons do not exist can be obtained simply by setting $\kappa_3=0$ in Eq. (A5).

Figure 19 shows several power-dispersion curves for TE plasmons in very thin metal-film structures of different thicknesses. For zero film thickness (the single-interface case) there is no upper-β cutoff point. As the metal-film thickness is increased the power threshold decreases and an upper-β cutoff appears. Since at the upper cutoff point the self-focused peak is at an infinite distance from the metal film and the field amplitudes in the metal and linear dielectric are zero, the power at the upper-β cutoff is carried entirely within the nonlinear medium, and is given analytically by the integral

$$\mathcal{P}_{\rm cutoff}=\frac{k}{2\omega\mu_0}\int_{-\infty}^{\infty}E_y^2 dz \tag{A6a}$$

$$=\frac{k\kappa_1^2}{2\omega\mu_0\Lambda}\int_{-\infty}^{\infty}\frac{dz}{\cosh^2(\kappa_1 z)} \tag{A6b}$$

$$=\frac{k\kappa_1}{\omega\mu_0\Lambda} , \tag{A6c}$$

which is independent of the data describing the metal film and linear dielectric. The locus of the power at cutoff given by Eq. (A6) is also shown in Fig. 19.

2. Dielectric layer

We consider the case where the dielectric layer has a higher dielectric constant than the bounding media, i.e., the usual linear guided modes exist. The nonlinear solutions in this case are well known for TE waves; Fig. 20 shows typical power-dispersion curves for TM_0 and TM_1 modes that are basically very similar to the corresponding TE modes.[11] The TM_0 mode degenerates into a self-focused single-interface wave as β is increased, but higher-order modes have a cutoff point as shown in the figure for the TM_1 mode. The cutoff point once again corresponds to the self-focused peak moving an infinite distance into the nonlinear medium, and can be obtained analytically in exactly the same way as for pseudoplasmons and TE plasmons.

[1]A. G. Litvak and V. A. Mironov, Izv. Vyssh. Uchebn. Zaved. **11**, 1911 (1968).
[2]M. Miyagi and S. Nishida, Rep. Res. Inst. Electr. Commun. Tohoku Univ. **24**, 53 (1972).
[3]W. J. Tomlinson, Opt. Lett. **5**, 323 (1980).
[4]A. A. Maradudin, Z. Phys. B **41**, 341 (1981).
[5]N. N. Akhmediev, Zh. Eksp. Teor. Fiz. **83**, 545 (1982) [Sov. Phys.—JETP **56**, 299 (1982)].
[6]A. D. Boardman and P. Egan, IEEE J. Quantum Electron. **QE-22**, 319 (1986).
[7]A. D. Boardman and P. Egan, IEEE J. Quantum Electron. **QE-21**, 1701 (1985).
[8]A. D. Boardman, P. Egan, and A. Shivarova, Appl. Sci. Res. **41**, 345 (1984).
[9]L. G. Bolshinskii and A. I. Lomtev, Pis'ma Zh. Tekh. Fiz. **11**, 358 (1985) [Sov. Tech. Phys. Lett. **11**, 148 (1985)].
[10]F. Lederer, U. Langbein, and H. E. Ponath, Appl. Phys. B **31**, 69 (1983).
[11]D. Mihalache and H. Totia, Solid State Commun. **54**, 175 (1985).
[12]C. T. Seaton, J. D. Valera, R. L. Shoemaker, G. I. Stegeman, J. T. Chilwell, and S. D. Smith, IEEE J. Quantum. Electron. **QE-21**, 774 (1985).
[13]G. I. Stegeman, C. T. Seaton, J. Ariyasu, R. F. Wallis, and A. A. Maradudin, J. Appl. Phys. **58**, 2453 (1985).
[14]T. Twardowski, Ph.D. thesis, University of Salford, 1988 (unpublished).
[15]A. D. Boardman, A. A. Maradudin, G. I. Stegeman, T. Twardowski, and E. M. Wright, Phys. Rev. A **35**, 1159 (1987).
[16]A. D. Boardman, T. Twardowski, A. Shivarova, and G. I. Stegeman, IEE Proc. J. **134**, 152 (1987).
[17]D. Mihalache, G. I. Stegeman, C. T. Seaton, E. M. Wright, R. Zanoni, A. D. Boardman, and T. Twardowski, Opt. Lett. **12**, 187 (1987).
[18]A. D. Boardman and T. Twardowski, in *Surface Plasmon Polaritons,* Proceedings of the Institute of Physics, London, 1988 (Institute of Physics, London, 1988).
[19]N. N. Akhmediev, Zh. Eksp. Teor. Fiz. **84**, 1907 (1983) [Sov. Phys.—JETP **57**, 1111 (1983)].
[20]V. M. Agranovich, V. S. Babichenko, and V. Ya. Chernyak, Pis'ma Zh. Eksp. Teor. Fiz. **32**, 532 (1980) [JETP Lett. **32**, 512 (1980)].
[21]C. T. Seaton, J. D. Valera, B. Svenson, and G. I. Stegeman, Opt. Lett. **10**, 149 (1985).
[22]J. Ariyasu, C. T. Seaton, G. I. Stegeman, A. A. Maradudin, and R. F. Wallis, J. Appl. Phys. **58**, 2460 (1985).
[23]A. G. Litvak and G. M. Fraiman, Zh. Eksp. Teor. Fiz. **68**, 1288 (1975) [Sov. Phys.—JETP **41**, 640 (1976)].
[24]T. P. Shen, G. I. Stegeman, and A. A. Maradudin, Appl. Phys. Lett. **52**, 1 (1988).
[25]A. D. Boardman and T. Twardowski, J. Opt. Soc. Am. B **5**, 523 (1988).
[26]P. N. Butcher, *Nonlinear Optical Phenomena* (Engineering Experiment Station, Ohio State University, 1965).
[27]U. Ascher, J. Christiansen, and R. D. Russell, ACM Trans. Math. Software **7**, 209 (1981).
[28]M. Fukui, V. C. Y. So, and R. Normandin, Status Solidi B **91**, K61 (1979).
[29]G. I. Stegeman, J. D. Valera, C. T. Seaton, J. Sipe, and A. A. Maradudin, Solid State Commun. **52**, 293 (1984).
[30]F. Lederer and D. Mihalache, Solid State Commun. **59**, 151 (1986).
[31]D. Mihalache, D. Mazilu, and F. Lederer, Opt. Commun. **59**, 391 (1986).